Journal of Luminescence 233 (2021) 117929

Contents lists available at ScienceDirect

Journal of Luminescence

journal homepage: http://www.elsevier.com/locate/jlumin

Laser-induced time-resolved luminescence in analysis of rare earth elements in apatite and calcite

Sari Romppanen [a,*], Heikki Häkkänen [b], Saara Kaski [a]

[a] Department of Chemistry, University of Jyväskylä, P.O. Box 35, FI-40014, Finland
[b] Department of Biological and Environmental Science, University of Jyväskylä, P.O. Box 35, FI-40014, Finland

ARTICLE INFO

Keywords:
Time-resolved spectroscopy
Apatite
Minerals
Calcite
Laser-induced luminescence
Rare earth elements

ABSTRACT

Laser-induced time-resolved luminescence was used to study rare earth element (REE) containing natural apatite and calcite minerals. The luminescence from 400 nm to 700 nm in the minerals was analyzed with excitation ranges 210–340 nm and 405–535 nm. As an outcome, several useful excitation wavelengths to detect one or more REE from apatite and calcite are reported. The feasibility of selected excitations in *e.g.* avoiding the disturbance of intense Mn^{2+} luminescence band, results was demonstrated with a non-gated detector.

1. Introduction

Rare earth elements (REEs) are representing a group of elements consisting of lanthanoids (La–Lu), yttrium (Y), and scandium (Sc). REEs are needed for modern technology [1] and a rapid analysis technique would be a benefit at many stages of their supply chain. REEs can act as luminescence centres in host minerals and therefore luminescence spectroscopy is efficient in detecting them. Natural minerals typically host several REEs simultaneously [2]. Although luminescence emission of REEs is generally observed as relatively sharp lines and only some ions *e.g.* Ce^{3+} and Eu^{2+} have broad bands [3], in natural minerals, the luminescence spectrum can be rather complex with several overlapping bands. For example, the crystal field of the host mineral lattice can split the energy levels of REE^{3+} ions [3] and as a consequence, more luminescence emission lines may appear. In addition, the intensity of luminescence emission is dependent on both the mineral's crystallinity and on the surroundings of the luminescence centre, which may change the energy transfer, quenching, reabsorption and sensitizing processes [4–6].

Although one of the most common techniques to luminescent mineral research is cathodoluminescence [7–11], laser-induced time-resolved luminescence spectroscopy has several benefits, *e.g.* high laser power excites also weak luminescence centres, time-resolving enables separation of different luminescence centres from each other and the method could be easily combined with other laser-spectroscopic method like Raman spectroscopy or laser-induced breakdown spectroscopy (LIBS), as reviewed in the literature [4,6,12–14]. However, the occurrence of luminescence is strongly dependent on the selection of the laser wavelength used for the excitation. Therefore, the aim of this research was to survey, which excitation wavelengths would be optimal for detecting luminescence of certain or multiple REEs. A tunable ns-pulse laser was used at excitation regions 210–340 nm and 405–535 nm to study luminescent minerals, apatite and calcite, from the same geological site. The emission was detected in the visible range, with a view to the possible *on-line* and *on-site* applications in the future. Based on the results, suggestions for optimal excitations for the detection of REEs were produced and the concept was tested using the laser with a basic non-gated spectrometer.

2. Materials & methods

Two natural mineral samples, apatite and calcite, were chosen from the Siilinjärvi ultramafic alkaline-carbonatite complex in Eastern Central Finland. At the Siilinjärvi complex REE-hosting minerals are occurring in the "glimmerite" (phlogopite rock) and carbonatite rock types [15,16]. REEs are known to be situated in Ca-bearing phases in carbonatites like carbonates and apatites and in previous research overall REE content is analyzed to be smaller in calcite (509 ppm in Mg-rich calcite in apatite sövite *i.e* carbonatite proper) than in apatite (2986 ppm in glimmerite and 3820 ppm in apatite sövite) [17]. The results enable the general assumption of the occurrence of the same REEs in the host lattice of the chosen samples. At the moment, apatite is

* Corresponding author.
E-mail address: sari.m.romppanen@jyu.fi (S. Romppanen).

https://doi.org/10.1016/j.jlumin.2021.117929
Received 10 June 2020; Received in revised form 15 January 2021; Accepted 18 January 2021
Available online 29 January 2021

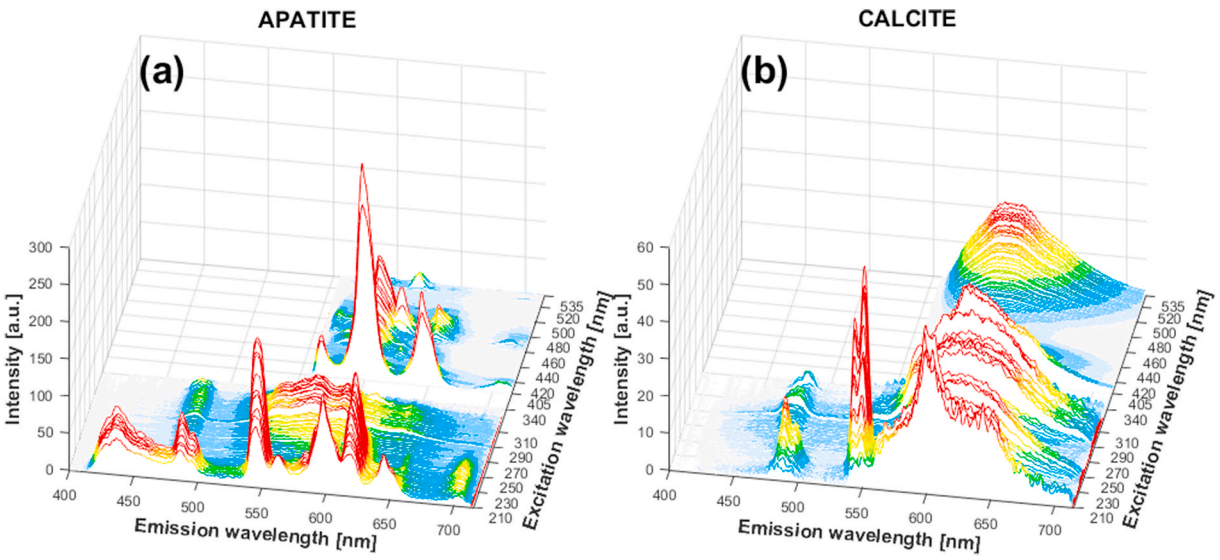

Fig. 1. Luminescence emission-excitation maps (EEMs) from apatite (a) and calcite (b), using excitations at UV (210–340 nm) and Vis (405–535 nm) with a step of 1 nm. The delay time was 50 μs and the gate 500 μs.

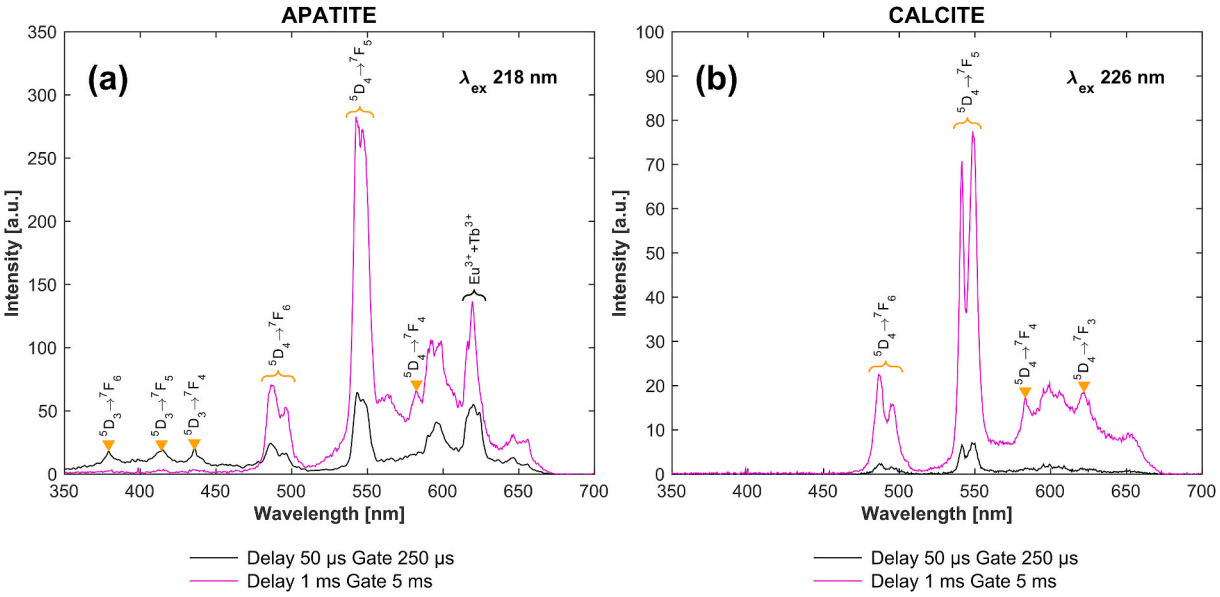

Fig. 2. The strongest luminescence peaks from Tb^{3+} (marked with orange triangles) can be observed at the laser excitation of 218 nm for apatite (a) and of 226 nm for calcite (b), measured at two different delay and gate times. Unmarked luminescence peaks are caused by Sm^{3+} and Eu^{3+}.

Table 1
Transitions and luminescence peaks of Tb^{3+} observed in apatite and calcite.

TRANSITION	APATITE [nm]	CALCITE [nm]
$^5D_3 \rightarrow {}^7F_6$	379	–
$^5D_3 \rightarrow {}^7F_5$	415	–
$^5D_3 \rightarrow {}^7F_4$	436	–
$^5D_4 \rightarrow {}^7F_6$	486/496	487/496
$^5D_4 \rightarrow {}^7F_5$	542	541/549
$^5D_4 \rightarrow {}^7F_4$	582	583
$^5D_4 \rightarrow {}^7F_3$	–	622

only exploited as a phosphate source [15]. Greenish apatite with a length about 2 cm representing medium-grained carbonate glimmerite and a 2 cm piece of reddish calcite were selected because they contained rather large areas of the same mineral macroscopically. Under a 254 nm ultraviolet (UV) lamp, both showed intense luminescence, especially calcite had a very strong red colour. The samples were sawed and polished.

Apatite often acts as a host to luminescent ions [18–21] and for example, manganese and REEs, can replace calcium in the mineral lattice. As the majority of apatite in Siilinjärvi complex is fluorapatite $Ca_5(PO_4)_3F$ [16], it is assumed that our sample is this phosphate mineral, having a hexagonal structure ($P6_3/m$) [22,23]. There are two Ca sites in the apatite's crystal structure: Ca (I) and Ca (II), which differ in both size and site-symmetry [9,18,22–24]. It is presented, how LREEs (light REEs: La–Sm) prefer the Ca (II) site in apatite's structure [25–28]. However, the REE content in apatite typically corresponds to the whole-rock composition, due to the poor REE selectivity [26,27,29]. Calcite's ($CaCO_3$) structure consists of planar carbonate $(CO_3)^{2-}$ groups within the centre of an equilateral oxygen triangle occupied by a carbon ion [18]. Rare earth elements can substitute Ca in calcite lattice and become luminescence centres, e.g. Refs. [4,6,12,30–34]. Also different divalent

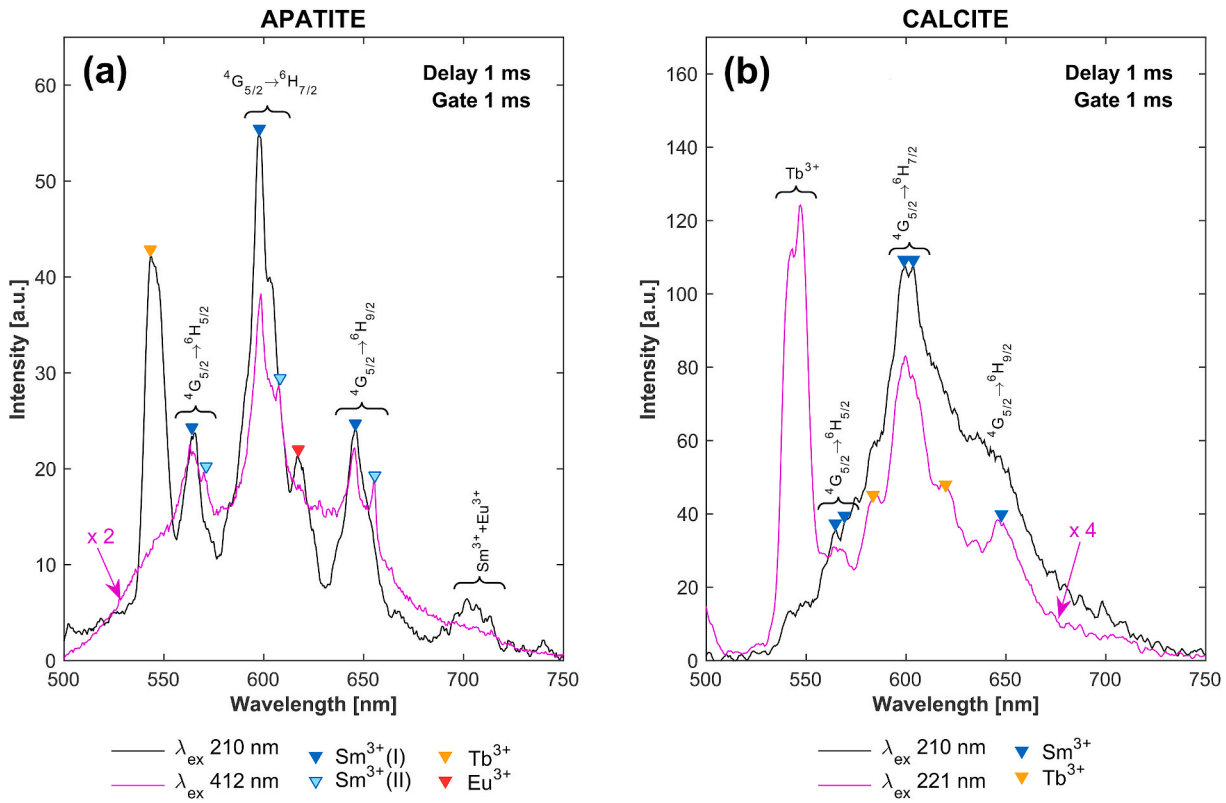

Fig. 3. In apatite (a) Sm^{3+} luminescence is observed only from substitution at Ca (I) site (dark blue triangles) or also from Ca (II) site (light blue triangles), depending on the excitation wavelength, here 210 nm (black) and 412 nm (violet), respectively. In calcite (b) the strongest Sm^{3+} signal is seen with excitation at 210 nm (black), but for other peaks of Sm^{3+}, the excitation at 221 nm (violet) is better. Note the scaling of the violet spectra in calcite. Peaks related to Tb^{3+} (orange triangles) and Eu^{3+} (red triangle) are also marked. All spectra were measured with a delay of 1 ms and a gate of 1 ms.

Table 2
Transitions and luminescence peaks of Sm^{3+} observed in apatite at two Ca sites and in calcite.

TRANSITION	APATITE: Ca (I) site [nm]	APATITE: Ca (II) site [nm]	CALCITE [nm]
$^4G_{5/2} \rightarrow {}^6H_{5/2}$	563	570	563/568
$^4G_{5/2} \rightarrow {}^6H_{7/2}$	598	607	599/604
$^4G_{5/2} \rightarrow {}^6H_{9/2}$	645	655	650
$^4G_{5/2} \rightarrow {}^6H_{11/2}$	705	–	–

cations can replace the Ca^{2+} cation, *e.g.* Mg^{2+}, Fe^{2+}, Mn^{2+} and Sr^{2+} [18].

Luminescence was measured with a home-built laser-induced time-resolved spectroscopy setup having a tunable laser wavelength system based on Ekspla OPO (optical parametric oscillator). The laser had a pulse duration of 3.3 ns and a repetition rate of 100 Hz. The signal was collected via a plano-convex lens with 45° geometry to the laser beam. The reflective collimator directed the light to fused silica fiber connected to the spectrograph. To block the laser light from the detector, a long-pass filter was used between the lens and reflective collimator. The selected filters had cut-on wavelengths at 266 nm, 400 nm, 450 nm, and 550 nm to match the excitation wavelengths between 210–340 nm and 405–535 nm. Each emission spectrum was accumulated from 400 laser pulses to average the influence of possible pulse-to-pulse laser energy fluctuations. All measurements were carried out at room temperature.

The light was directed to the Czerny-Turner type imaging spectrograph (Acton, SP-150) equipped with a grating having 300 grooves per mm (blazed to 500 nm, resolution >1 nm) and spectra were recorded with ICCD (Instaspec V, Oriel). The spectral range was about 350 nm and the central wavelength was changed by turning the grating. The calibration was carried out with HgAr lamp. A delay generator (model DG 535, Stanford Research System, Inc.) was used to control the time parameters of ICCD. To exclude the broad, strong, and very short-living luminescence emission bands of Ce^{3+} and Eu^{2+}, which are known to dominate steady-state luminescence spectra [6,35,36], a delay of 50 μs was used in the measurement of excitation-emission maps (EEMs) of calcite and apatite. The luminescence lifetimes (τ) of Ce^{3+} and Eu^{2+} bands are presented to be < 1 μs in literature, *e.g.* Ref. [6] and the chosen delay was proven also experimentally to be suitable for exclude these. Spectra were measured with a step of 1 nm (laser wavelength). Gate width was 500 μs to avoid the dominance of the long-living luminescence peaks. The benefit of the time-gated detection is presented on supplementary material (Fig. A1) with excitation wavelength of 266 nm. To further analyse the observed REE^{3+} emissions, certain wavelengths were re-measured with different delay times (10 μs, 50 μs, and 1 ms) with varying gate widths (25 μs, 250 μs, 1 ms, and 5 ms).

To test the predicted optimal excitation wavelength areas, the luminescence signal was directed to a non-gated Czerny-Turner type CCD spectrometer (Thorlabs, model CCS200, grating 600 lines/mm; blazed to 800 nm and FWHM spectral accuracy < 2 nm). The spectral range was 200–1000 nm, and the filters were applied to block the excitation laser light.

Data processing was carried out with MathWorks MATLAB R2015a program. As the laser energy varies in OPO as a function of wavelength, it was compensated for each spectrum by dividing the spectral intensities by the average energy value measured with Ophir (model PE10-SH-V2) laser power meter. All presented spectra have slight smoothing for enhanced visualization.

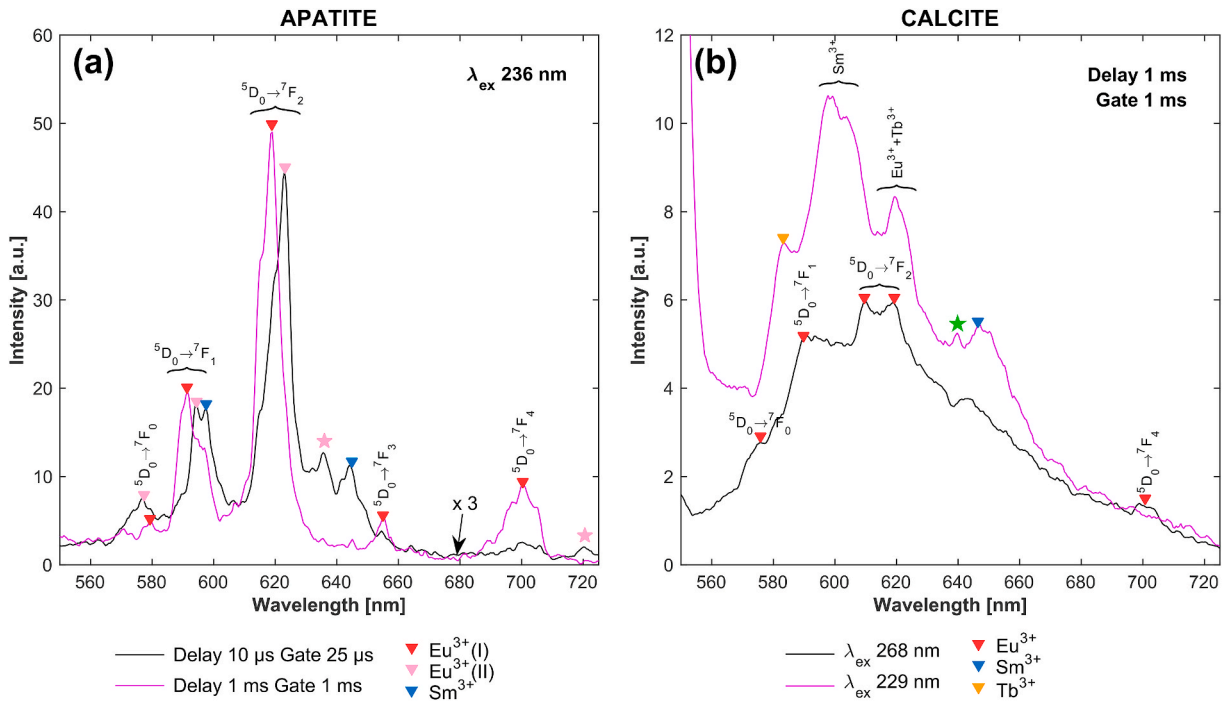

Fig. 4. In apatite (a) Eu^{3+} luminescence peaks from Ca (I) and Ca (II) sites can be observed with the same excitation wavelength of 236 nm by changing the delay time. Emission of Eu^{3+} in Ca (II) site can be seen with the shorter delay (10 µs, black) and emission of Eu^{3+} in Ca (I) site with the longer delay (1 ms, violet). In calcite (b) either the strong background caused by the Mn^{2+} band at excitation of 268 nm (black) or emission peaks from other REEs disturb the detection of Eu^{3+} luminescence (violet). Both spectra of calcite were measured with a delay of 1 ms and a gate of 1 ms. The peaks of Sm^{3+} (blue triangle) and Tb^{3+} (orange triangles) are marked in spectra and the peak with a green star in calcite is possibly related to Pr^{3+}.

Table 3
Eu^{3+} luminescence peaks recognized in apatite's Ca sites and in calcite, with respective transitions.

TRANSITION	APATITE: Ca (I) site [nm]	APATITE: Ca (II) site [nm]	CALCITE [nm]
$^5D_0 \rightarrow {}^7F_0$	579	573, 577	577
$^5D_0 \rightarrow {}^7F_1$	591	595	591
$^5D_0 \rightarrow {}^7F_2$	618	623	610/620
$^5D_0 \rightarrow {}^7F_3$	655	–	–
$^5D_0 \rightarrow {}^7F_4$	700	–	702

3. Results & discussion

3.1. Laser-induced time-resolved luminescence of apatite and calcite

Time-resolved luminescence spectra from apatite and calcite were measured at a range of 400–700 nm using excitations 210–340 nm and 405–535 nm. The delay time was 50 µs and the gate width 500 µs. Excitation-emission maps (EEMs) are shown in Fig. 1.

The chosen delay and gate times seem to be suitable for observing several narrow REE^{3+} luminescence peaks simultaneously. Shape of spectrum varies as the excitation wavelength changes. Intensities of the luminescence peaks and bands in calcite were lower than in apatite, which is most likely caused by the lower REE content in calcite in the Siilinjärvi [17].

In apatite (Fig. 1a) more REE^{3+} peaks can be observed than in calcite (Fig. 1b), where a broad luminescence band around 620 nm is dominating spectra at wide excitation regions. This band is caused by Mn^{2+} and is thoroughly studied, *e.g.* Refs. [8,30,37–43]. Also, the broad Mn^{2+} band is peaking at 573 nm in apatite (Fig. 1a) – note that the change in the emission wavelength is caused by different mineral structures [8]. In literature Mn^{2+} band in apatite in this spectral region has been observed earlier [21,44] and Mn^{2+} can accommodate both Ca (I) and Ca (II) sites in apatite's structure [4,19,45]. The absolute intensity of Mn^{2+} band in the measured excitation wavelength regions has no considerable difference between the apatite and calcite, even though the relative intensities of Mn^{2+} and REE^{3+} luminescence between the minerals differ (Fig. 1). Calcite from Siilinjärvi contains typically 0.10–0.32 wt % of MnO, whereas apatite has only 80–300 ppm of Mn [16]. In order to study how REEs contribute to the EEMs in Fig. 1, in the following selected excitation wavelengths are discussed in detail.

At excitation wavelength 218 nm, a strong double peak at 542 nm is observed in apatite (Fig. 2a) which is assigned as Tb^{3+} luminescence transition $^5D_4 \rightarrow {}^7F_5$ [4,7,12,46–60]. In calcite, this peak is detected at 541/549 nm and the strongest intensity is obtained at excitation wavelength 226 nm (Fig. 2b). The different mineral structures can explain the difference in both locations and relative intensities of this Tb^{3+} peak. Also, Tb^{3+} transitions $^5D_4 \rightarrow {}^7F_6$ and $^5D_4 \rightarrow {}^7F_4$ are seen in both minerals: at 486/496 nm and 582 nm in apatite (Fig. 2a) and 487/496 nm and 583 nm in calcite (Fig. 2b). In apatite also Tb^{3+} peaks at 379 nm, 415 nm and 436 nm can be detected, but only with measurement of delay 50 µs (Fig. 2a, black) and the respective transitions in the literature are $^5D_3 \rightarrow {}^7F_6$, $^5D_3 \rightarrow {}^7F_5$ and $^5D_3 \rightarrow {}^7F_4$ [4,7,36,48,52,57,59,60]. The different mineral lattice may cause the absence of these peaks in calcite, as the host material has been observed to influence the intensity of certain Tb^{3+}peaks [4,12]. Tb^{3+} has a transition of $^5D_4 \rightarrow {}^7F_3$, typically observed around ~620 nm, depending on the host material [46–49,55, 57–59]. In calcite, it is observed at 622 nm with the measurement delay of 1 ms (Fig. 2b, violet), but in apatite, there is a strong contribution from nearby Eu^{3+} peaks and the exact location of Tb^{3+} transition cannot be pointed. All clearly observed luminescence peaks of Tb in calcite and apatite and the respective transitions are collected into Table 1.

Several strong Sm^{3+} luminescence peaks can be seen in both minerals. In apatite Sm^{3+} can occupy Ca (I) and Ca (II) sites in the mineral structure [4,6,9,12,19,36,61,62]. For example, Sm^{3+} luminescence at excitation wavelength of 210 nm originates from the substitution to Ca (I) site (Fig. 3a, black). When excitation is changed to 412 nm (Fig. 3a,

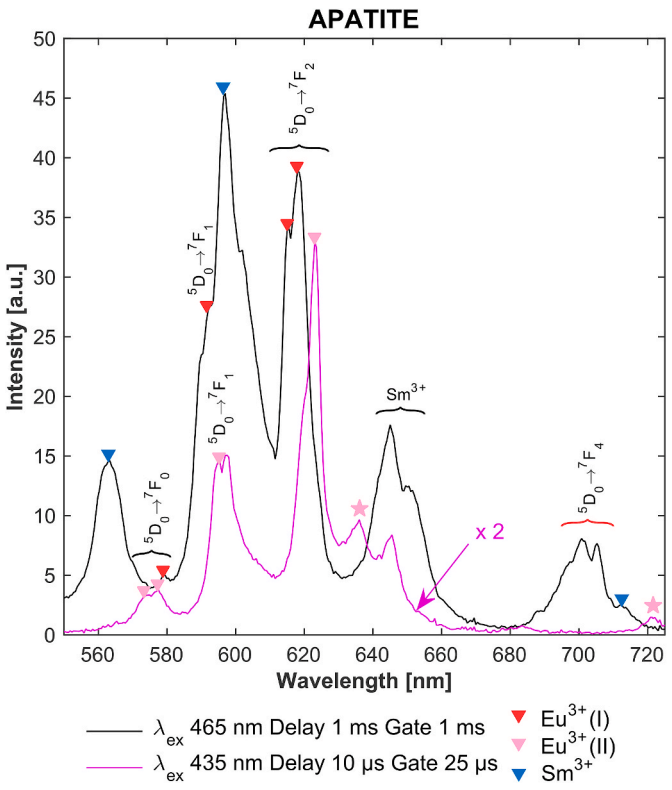

Fig. 5. Visible excitations can be used for detection of Eu^{3+} luminescence in apatite because the Mn^{2+} band is not detected in this excitation region. As an example, Eu^{3+} in Ca (I) site (red triangles) is better observed with excitation 465 nm (black) whereas Eu^{3+} in Ca (II) site (pink triangles) is seen with 435 nm excitation wavelength (violet). The measurement delay for observing luminescence from the sites is different, the longer 1 ms for Eu^{3+} in Ca (I) site, and the shorter 10 µs for Eu^{3+} in Ca (II) site. Note the scaling of the violet spectrum.

violet), also luminescence from Ca (II) site is detected. The band ~700 nm in apatite is a combination of Eu^{3+} and Sm^{3+} transition $^4G_{5/2} \rightarrow {}^6H_{11/2}$ (Fig. 3a, black).

In calcite the strongest Sm^{3+} luminescence was observed with excitation at 210 nm, but also a broad Mn^{2+} band occurs, nearly hindering the detection of other Sm^{3+} peaks than the double peak at 599/604 nm (Fig. 3b, black). At excitation 221 nm, also peaks at 563/568 nm and 650 nm can be detected clearly (Fig. 3b, violet). The occurrence of Sm^{3+} luminescence as two double peaks have also been reported for synthetic calcites [30,43,63,64]. Due to the strong luminescence of the overlapping Mn^{2+} band, the used visible excitations are not relevant for successful detection of Sm^{3+} in the measured calcite. All observed Sm^{3+} luminescence peaks are collected in Table 2 with the respective transitions recognized via literature [53,58,65–73].

Analogous to samarium, also luminescence of Eu^{3+} has been observed from different Ca sites in apatite, *e.g.* Refs. [9,19,36,74–86]. This is also the case in our study and as an example, spectra measured with excitation 236 nm are presented (Fig. 4a). The appearance of the luminescence from two Ca sites can be controlled by changing the delay time of the measurement. At the shorter delay of 10 µs, luminescence peaks of Eu^{3+} in Ca (II) site can be observed at 577 nm, 595 nm, and 623 nm (Fig. 4a, black). With the longer measurement having the delay of 1 ms, the luminescence from Eu^{3+} in Ca (I) site can be observed in 579 nm, 591 nm, 618 nm, 655 nm and 700 nm (Fig. 4a, violet). The peak ~620 nm is rather wide regardless of the occupied Ca site, which suggests further fine structure within this peak. It can be noted that we observe peaks at 636 nm and 720 nm in apatite (pink stars in Fig. 4a), always when also the peaks of Eu^{3+} from Ca (II) site are seen. Our assumption is, that both are luminescence of Eu^{3+} in Ca (II) site, somewhat supported by previous research, where the peak observed at ~636 nm was explained as a vibronic transition of Eu^{3+} in Ca (II) site [76,86].

In calcite, the detection of Eu^{3+} peaks is challenging due to the broad and strong Mn^{2+} band, as they are excited simultaneously. With excitation wavelength 268 nm, luminescence of Eu^{3+} is observed at 577 nm, 591 nm, 610 nm, 620 nm, 655 nm, and 702 nm although there is also Mn^{2+} band underneath (Fig. 4b, black). It can be remarked, that the transition $^5D_0 \rightarrow {}^7F_2$ here is observed as a double peak at 610/620 nm, also reported for doped calcite samples [43,63,87,88]. When luminescence from calcite is measured with excitation 229 nm, the contribution of Mn^{2+} is also relatively low and only the Eu^{3+} peak at 620 nm is seen along the adjacent Tb^{3+} peak (Fig. 4b, violet), whereas other Eu^{3+} peaks are not resolved. Table 3 summarizes the observed Eu^{3+} luminescence peaks in both minerals and the corresponding transitions were recognized based on *e.g.* Refs. [49,67,89–92].

We assume, that peak at 641 nm in calcite (Fig. 4b, green star) might be related to Pr^{3+}, which is observed around this spectral region [61,62,71,93–95]. Also, the suitability of deep UV excitation for Pr^{3+} in minerals has been proved very recently [96]. However, in the scope of this study, the occurrence of Pr^{3+} in our sample cannot be proven, because the other intensive Pr^{3+} peaks in this spectral region are located around 600 nm and most likely be overwhelmed by strong Sm^{3+} luminescence and by Mn^{2+} in calcite.

In the above, the occurrence of Eu^{3+} luminescence was only presented with UV excitation. In apatite, where the Mn^{2+} luminescence was not as strong as in calcite, the Eu^{3+} peaks can also be efficiently observed using also visible excitation. For example, excitation at ~465 nm is suitable for detecting Eu^{3+} in Ca (I) site whereas ~435 nm is good for Eu^{3+} in Ca (II) site (Fig. 5). The measurement times are analogous to our previous observations; the luminescence of Eu^{3+} from Ca (I) site is strong at the longer delay (1 ms) whereas from Ca (II) it is better observed at the shorter delay time (10 µs). In Fig. 5 those Eu^{3+} transitions, which have a strong contribution of nearby Sm^{3+} luminescence, are not marked. At excitation 435 nm there are two peaks related to transition $^5D_0 \rightarrow {}^7F_0$ at 573 nm and 577 nm (Fig. 5, violet). Therefore, it is assumed that in our sample Eu^{3+} is occupying at least three different Ca sites because europium's states $^5D_0$ and $^7F_0$ are non-degenerated [82]. It can be also remarked that the same peaks at 636 nm and 720 nm (Fig. 5, pink stars), which were seen in Fig. 4a along with the Eu^{3+} occurrence in Ca (II) site in apatite's structure are observed here as well.

The two strongest Dy^{3+} bands can be seen at ~480 nm and ~575 nm in both apatite and calcite *e.g.* with excitation 427 nm (Fig. 6). The corresponding transitions are $^4F_{9/2} \rightarrow {}^6H_{15/2}$ and $^4F_{9/2} \rightarrow {}^6H_{13/2}$ also reported previously for various dysprosium containing samples [69,73,90,97–100]. The recognized Dy^{3+} peaks are presented in Table 4. The peak at ~480 nm is wide and seems to consist of several peaks located very close together in both minerals. Such fine structure for the Dy^{3+} peak has been reported on apatite [61], in doped calcites [43,63] and other materials [7,100]. It seems that in apatite (Fig. 6a) the relative intensities of three peaks at 475 nm, 480 nm, and 484 nm vary when the measurement delay is changed from 10 µs to 1 ms, but such behaviour is not observed in calcite (Fig. 6b). We anticipate that this could be caused by the Dy^{3+} occupying different Ca sites in apatite, which would lead to the difference in relative intensities at changed delays, as demonstrated earlier for Eu^{3+}.

The Dy^{3+} band at ~575 nm is clearly observed with excitation 452 nm for apatite and 454 nm for calcite (Fig. 6, cyan). Also here is the fine structure of closely located peaks and similar patterns have been presented for Dy^{3+} at ~575 nm by others, *e.g.* Refs. [7,61,77]. With the excitation wavelength of 427 nm, the Dy^{3+} ~575 nm luminescence is strongly contributed by other luminescence species. In apatite adjacent Eu^{3+} (II) peak is dominating at the shorter measurement delay 10 µs (Fig. 6a, black). If the delay is changed to 1 ms, Dy^{3+} at 578 nm in apatite nm can be better resolved, but there is a background from the Mn^{2+}, Sm^{3+} (I), and Sm^{3+} (II) (Fig. 6a, violet). In calcite, the Dy^{3+} peak at 579 nm can be observed at the shorter delay only, as at the longer

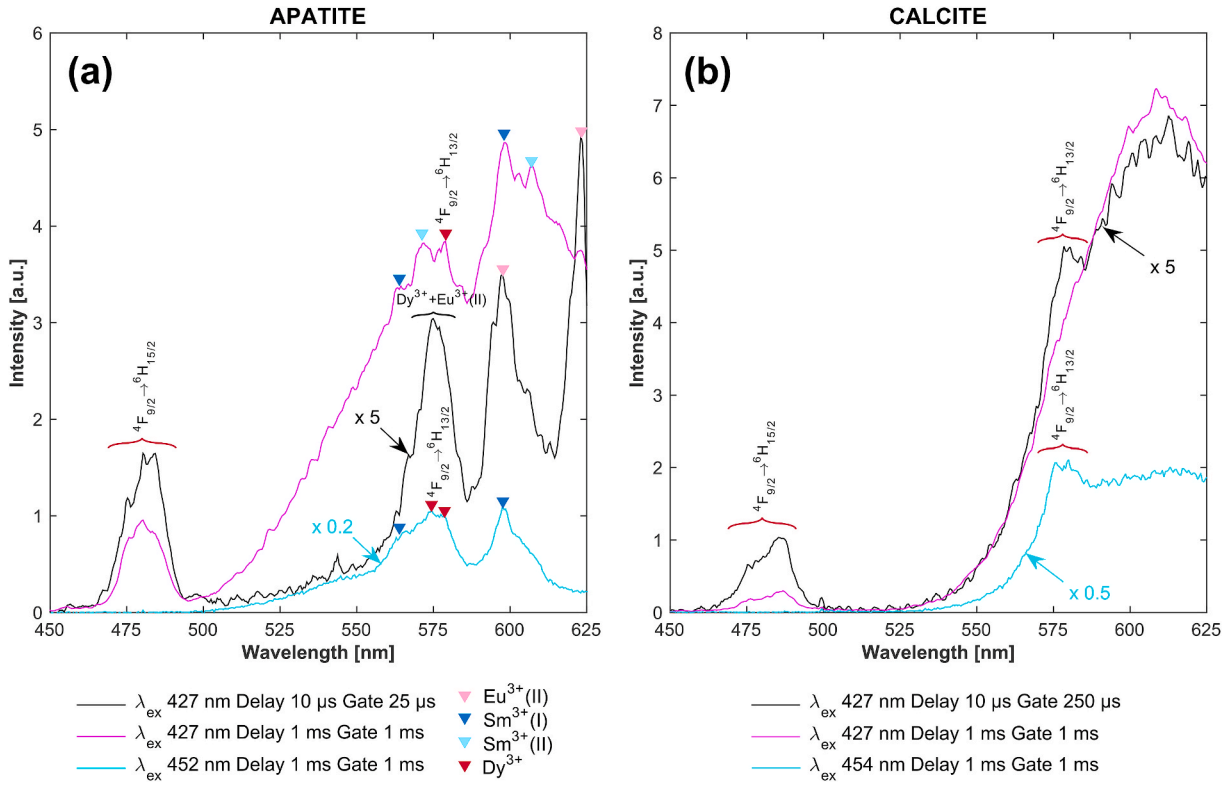

Fig. 6. Dy^{3+} luminescence peaks ~480 nm and ~575 nm in apatite (a) and calcite (b). The peak at 575 nm Dy^{3+} is observed clearly with excitation 452 nm (cyan), as laser wavelength 427 nm induces luminescence to the same spectral region also from other REEs and Mn^{2+}, which is demonstrated with measurement delays of 10 µs and as 1 ms (black & violet). Note the scaling of the black and the cyan spectra.

Table 4
Transitions and luminescence peaks of Dy^{3+} observed in apatite and calcite.

TRANSITION	APATITE [nm]	CALCITE [nm]
$^4F_{9/2} \rightarrow {}^6H_{15/2}$	475/480/484	485
$^4F_{9/2} \rightarrow {}^6H_{13/2}$	574/578	576/579

delays it is overwhelmed by intense Mn^{2+} band.

The right selection of the measurement time parameters with excitation 427 nm has importance in discovering the Dy^{3+} band at ~575 nm. In apatite, at the measurement of delay 10 µs, Dy^{3+} has a strong contribution of Eu^{3+} (II) peak (Fig. 6a, black). Measurement performed with the longer delay (1 ms), the Dy^{3+} at 578 nm in apatite nm can be better resolved (Fig. 6a, violet), but a strong contribution of Mn^{2+}, as well as Sm^{3+} (I) and Sm^{3+} (II), can be seen. In calcite (Fig. 6b), the detection of Dy^{3+} peak at 579 nm can be observed at the shorter delay

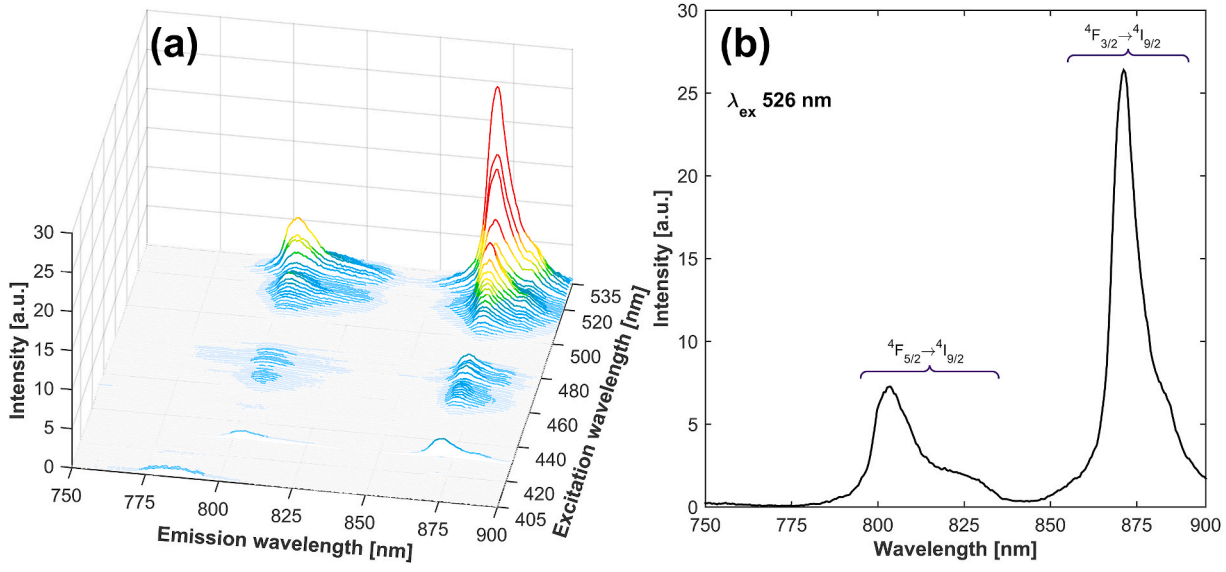

Fig. 7. Luminescence emission-excitation map from apatite (a) using excitations at 405–535 nm with a step of 1 nm. The Nd^{3+} luminescence peaks and the corresponding transitions are presented with excitation 526 nm (b). The delay time was 50 µs and gate width 500 µs in the measurements.

Table 5
Transitions and luminescence peaks of Nd^{3+} observed in apatite.

TRANSITION	APATITE [nm]
$^4F_{5/2} \rightarrow {}^4I_{9/2}$	804
$^4F_{3/2} \rightarrow {}^4I_{9/2}$	871

only, as at the longer delays the luminescence is overwhelmed by intensive Mn^{2+} band.

In the above, the luminescence emission in the visible spectral region was presented. In addition to it, also Nd^{3+} luminescence in the spectral region of 750–900 nm was measured. As observed in EEM of apatite, measured with excitation from 405 nm to 535 nm (Fig. 7a), the strongest intensities of Nd^{3+} bands are seen at excitation 526 nm. The Nd^{3+} luminescence bands are located at ~790–835 nm and ~850–940 nm, having the highest peaks at 804 nm and 871 nm, respectively (Fig. 7b, Table 5). Corresponding transitions are stated in the literature as $^4F_{5/2} \rightarrow {}^4I_{9/2}$ [7,101,102] and $^4F_{3/2} \rightarrow {}^4I_{9/2}$ [7,69,98,101–107]. Under the same measurement conditions (delay 50 μs and gate width 500 μs) no Nd^{3+} peaks were detected in calcite, which is most likely explained by the lower REE content in calcite than apatite at the Siilinjärvi complex.

3.2. Selection of optimized excitation wavelengths for apatite and calcite

The appearance of the luminescence spectrum depends significantly on the excitation wavelength. This is efficiently visualized as animations for excitation in the UV (video B1) and the visible (video C1) range. Normalization offers better comparison of the changed spectral shapes, thus the intensity values of apatite and calcite are normalized to the maximum of respective spectrum. The delay time in the measurements was 50 μs and the gate width 500 μs. For further applications in the luminescence analysis of natural minerals, it is useful to know which excitation wavelengths can be used to separate specific REEs or, on the other hand, to observe multiple REE^{3+} peaks simultaneously. Therefore, the laser-induced time-resolved luminescence spectra measured from apatite and calcite (Fig. 1) are illustrated as 2D contour presentations of EEMs (Figs. 8–10). The excitation regions (UV, Vis) are shown separately and for clarity, only the locations of the most prominent REE^{3+} peaks are marked as dashed lines. Deviating from Fig. 1, Contour EEM of apatite in the visible excitation region (Fig. 8), shows also spectral area of 750–900 nm presented in Fig. 7.

Contour-EEM of apatite in the visible excitation region shows luminescence from several REEs and no significant contribution of the Mn^{2+} band is observed (Fig. 8). The highest intensities for the Dy^{3+} peak at 578 nm are obtained with excitations at 427 nm and 452 nm. All the excitation wavelength regions, where Dy^{3+} is detected clearly, here 424–429 nm and 444–458 nm, are presented as grey boxes on the left side of the map, and stars show the most suitable excitations in our study. The same notation is used throughout all EEMs. Eu^{3+} can be excited from apatite using several spectral regions. With the delay of 50 μs luminescence from both mineral sites is seen and to separate Eu^{3+} peaks, those related to Ca (II) site are marked with pink. The good excitation wavelength for Eu^{3+} in apatite's Ca (I) site is 465 nm and for Eu^{3+} in Ca (II) sites either 435 nm, 473 nm, or 527 nm Sm^{3+} peaks have high intensities in apatite at wide excitation range. At Ca (I) site Sm^{3+} is well observed at excitations 405 nm and 473 nm. If also Sm^{3+} at Ca (II) site should be measured, the highest intensities were obtained with 414 nm excitation, marked with a pink star. The other REEs do not disturb the detection of Nd^{3+} peaks and in this research, the excitation 526 nm was the best.

In the apatite's EEM in UV excitation region (Fig. 9), background from some shorter living luminescence is here seen around the Tb^{3+} peaks (see also Fig. 1a), but they are clearly resolved and the highest intensities are obtained at 218 nm. The broad and intense Mn^{2+} band ~575–650 nm disturbs the detection of the other REEs, especially at excitations from 275 to 320 nm. The strongest intensities for Dy^{3+} peaks were observed at excitations of 287 nm and 326 nm. For Eu^{3+} the most suitable excitation wavelength at UV was 236 nm and the Sm^{3+} peak offered a strong signal when 210 nm was used for the excitation.

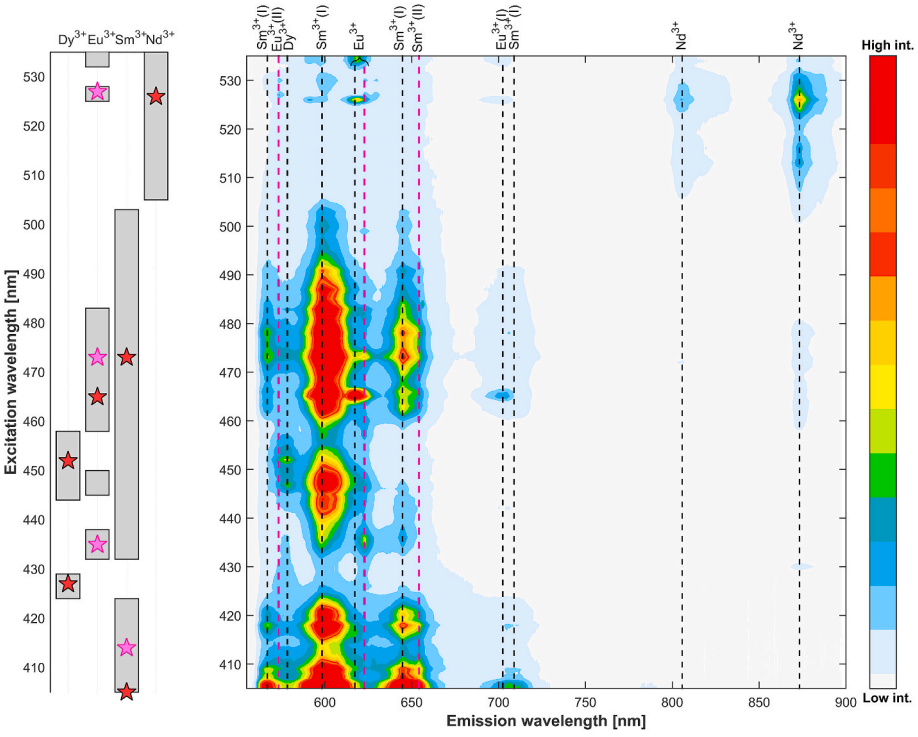

Fig. 8. Contour presentation of the excitation wavelengths in the visible for apatite as a function of luminescence emission wavelength (EEM-Vis). Locations of the selected REE^{3+} peaks are marked with black dashed lines and the appearance in Ca (II) site for Eu^{3+} and Sm^{3+} are marked with pink colour. The prominent excitation wavelengths are marked as grey boxes on the left side and the suggestions for optimal excitations are presented with stars.

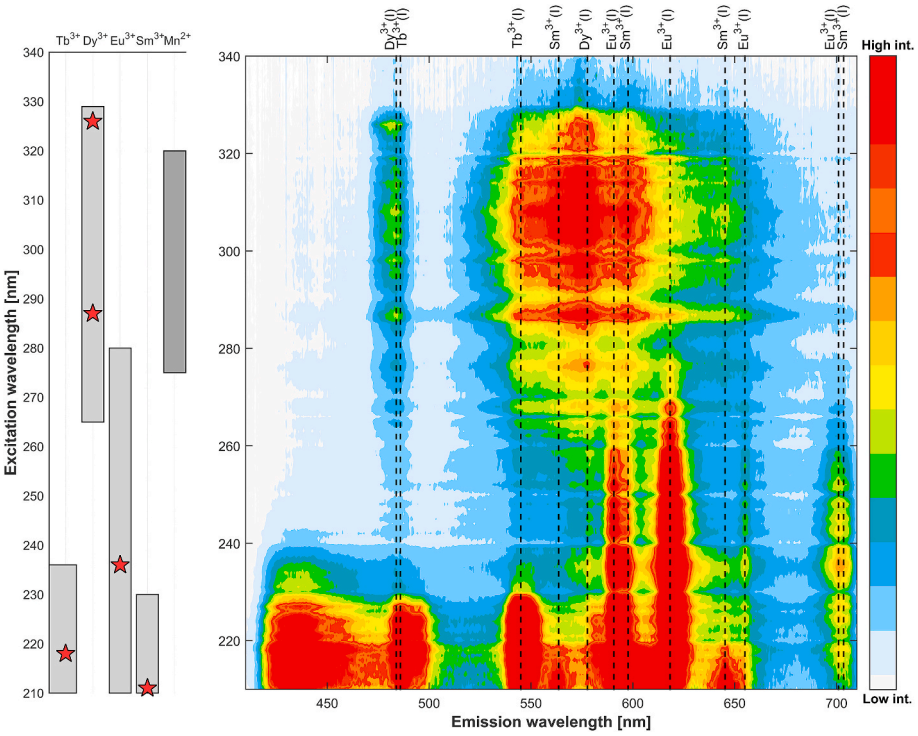

Fig. 9. Contour presentation of the excitation wavelengths in the UV for apatite as a function of luminescence emission wavelength (EEM-UV). Locations of the selected REE^{3+} peaks are marked with black dashed lines and suitable excitation wavelengths are marked as grey boxes on the left side of the contour and the suggestions for optimal excitations are presented with stars.

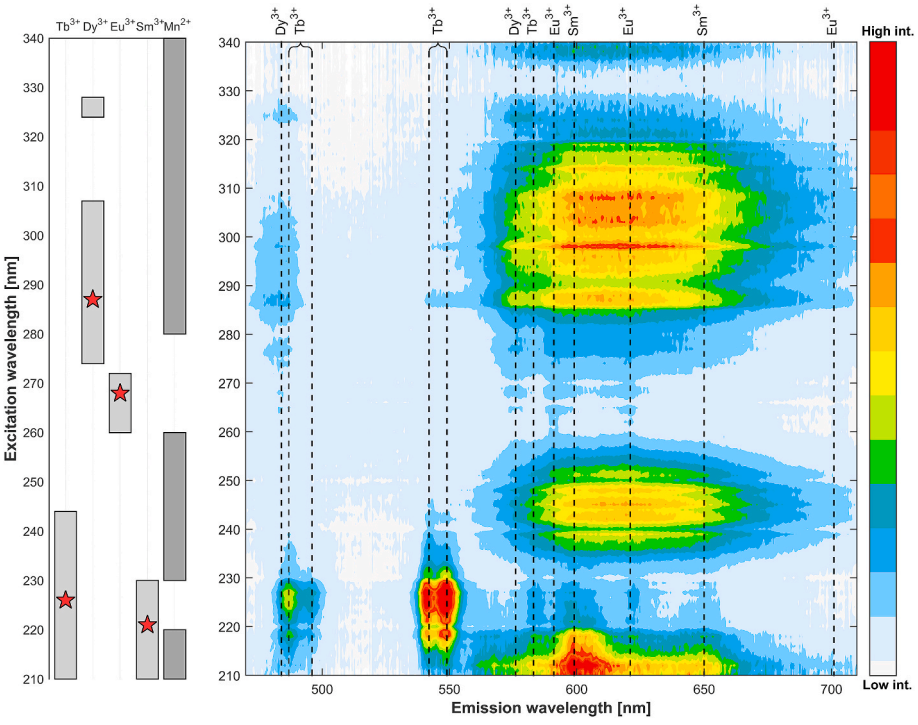

Fig. 10. Contour presentation of the excitation wavelengths in the UV for calcite as a function of luminescence emission wavelength (EEM-UV). The broad band of Mn^{2+} luminescence is observed ~575–650 nm at several excitation ranges. Locations of the selected REE^{3+} peaks are marked with black dashed lines. The prominent excitation wavelengths are marked as grey boxes on the left side and the suggestions for optimal excitations are presented with stars.

In calcite, the visible excitations strongly induce luminescence of Mn^{2+} and it readily dominates the spectra, as demonstrated in Fig. 1b. As an exception, the excitation 454 nm is applicable to Dy^{3+} and excitation 405 nm for the Sm^{3+}, but both have a notable background. For this reason, the contour-EEM for calcite is only presented in the UV excitation range (Fig. 10). For Tb^{3+} luminescence, the best excitation is at 226 nm. Because of Mn^{2+}, for the other REE^{3+} peaks the optimal excitation ranges (grey boxes) in calcite are not as wide as was shown for

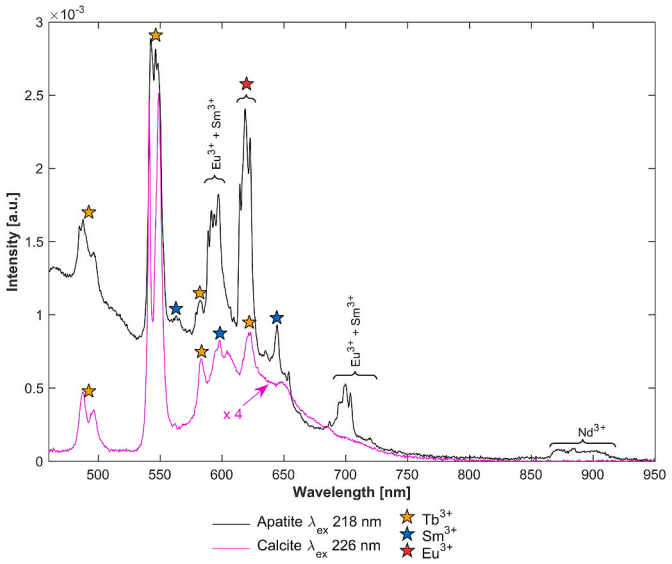

Fig. 11. Non-gated laser-induced luminescence measurements with the best excitations for Tb^{3+} for apatite (λ_{ex} 218 nm, black) and calcite (λ_{ex} 226 nm, violet). The Tb^{3+} peaks are marked with orange stars, Sm^{3+} as blue stars and Eu^{3+} as a red star. Note scaling of the violet spectrum.

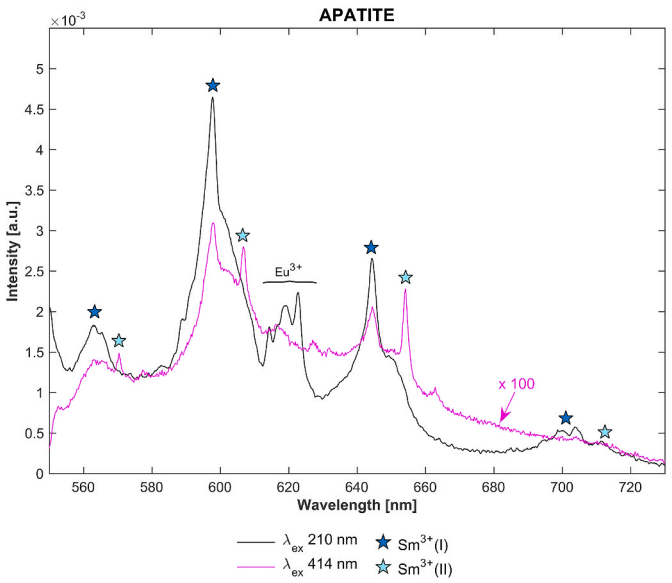

Fig. 12. Non-gated laser-induced luminescence measurements demonstrate how the optimal selection of excitation wavelength can show either only from Sm^{3+} in Ca (I) site (λ_{ex} 210 nm, black with blue stars) or also from Ca (II) site (λ_{ex} 414 nm, violet with blue and light blue stars). With excitation 210 nm also Eu^{3+}peaks are observed. Note the scaling of the violet spectrum.

apatite. The excitation of 287 nm is applicable to Dy^{3+} peaks and for Eu^{3+} and Sm^{3+} the excitations 268 nm and 221 nm, respectively, were found good.

The results offer possibility to locate those excitation wavelengths, where the emission signal of one or several REE^{3+} peaks are intensive and the disturbance of Mn^{2+} luminescence is minimal. The applicability was tested by measuring luminescence with a non-gated spectrometer with a few selected excitation wavelengths from the same samples. Without time-gating the long-living Mn^{2+} luminescence could readily dominate the spectrum even at low concentrations of Mn. However, the relative intensities of the REE peaks will not be comparable due to the varying lifetimes of the luminescence activators.

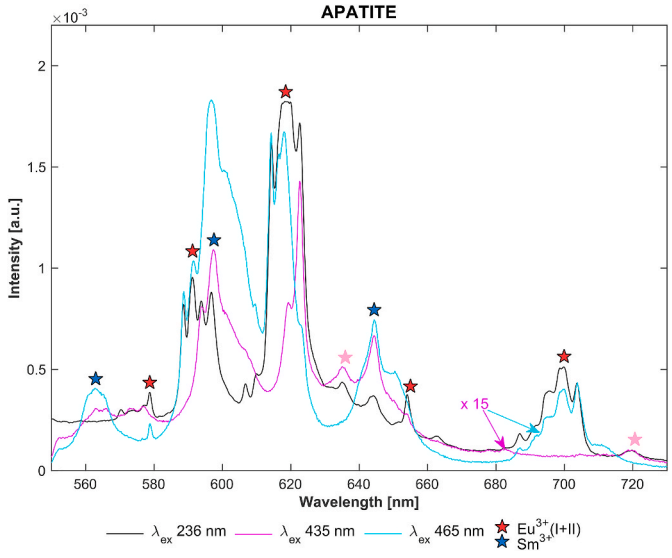

Fig. 13. Non-gated laser-induced luminescence measurements show peaks of Eu^{3+} (red stars) in apatite's Ca (II) site (λ_{ex} 435 nm, violet), Ca (I) site (λ_{ex} 465 nm, cyan) and on both of these sites (λ_{ex} 236 nm, black). Note the scaling of violet and cyan spectra. Sm^{3+} peaks are marked as blue stars.

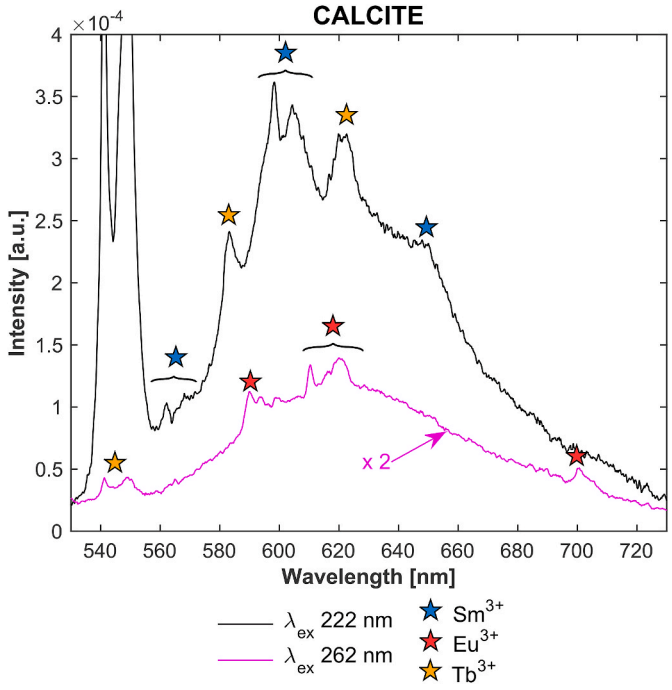

Fig. 14. Laser-induced non-gated luminescence measurements of calcite show the peaks of Tb^{3+} and Sm^{3+} (λ_{ex} 236 nm, black) and of Eu^{3+} (λ_{ex} 262 nm, violet). Note the scaling of the violet spectrum.

Firstly, the optimal excitations of Tb^{3+} for calcite and apatite were measured (Fig. 11). At these deep UV excitation wavelengths, both spectra show the luminescence peaks of Tb^{3+} and Sm^{3+} clearly (orange and blue stars), despite the background caused by the luminescence of Eu^{2+}, Ce^{3+}, and Mn^{2+}. In apatite (Fig. 11, black) also several Eu^{3+} related peaks (red star) and the Nd^{3+} band are seen.

Secondly, the occurrence of Sm^{3+} in both Ca (I) and Ca (II) sites in apatite's structure was measured. Luminescence of Sm^{3+} in the Ca (I) site can be detected in many excitation areas and here UV excitation 210 nm was selected (Fig. 12, black). Several peaks of Sm^{3+} in Ca (I) site

(blue stars) can be observed in addition to the luminescence peaks of Eu^{3+} occupying both sites. If also Sm^{3+} in Ca (II) is needed, the excitation at 414 nm (Fig. 12, violet) shows intensive luminescence peaks (light blue stars).

Eu^{3+} was also observed in the time-resolved measurements to occupy Ca (I) and Ca (II) sites in apatite, but optimal delay times were varying. In the non-gated measurement, the influence of the excitation wavelength seems to be decisive (Fig. 13). At excitation 236 nm (Fig. 13, black) the luminescence of Eu^{3+} is seen from Ca (I) and Ca (II) sites (red star). For comparison, excitation wavelength 435 nm shows Eu^{3+} peaks from Ca (II) site (Fig. 13, violet) and excitation 465 nm from Ca (I) site (Fig. 13, cyan). It can be remarked that the peaks at 636 nm and 720 nm (pink stars) are observed also here when the luminescence of Eu^{3+} from Ca (II) site is induced. This supports our assumption, that these peaks are related to Eu^{3+} and especially to Ca (II) site. Sm^{3+}peaks are seen in all spectra of Fig. 13.

For non-gated measurements of calcite, only UV excitations were used, as the luminescence of Mn^{2+} was strong already in the time-resolved study. Even with the selected UV excitations 222 nm and 262 nm, the background caused by Mn^{2+} in calcite is notable (Fig. 14). With excitation of 222 nm strong peaks of Sm^{3+} and Tb^{3+} are seen (Fig. 14, black). For non-gated measurement of Eu^{3+} in calcite, the excitation 262 nm seems to be the best (Fig. 14, violet).

4. Conclusion

The aim of the research was to study how REEs could be efficiently detected in natural apatite and calcite by optimizing the laser excitation wavelength. Luminescence from both minerals was systematically measured using excitations of 210–340 nm and 405–535 nm with tunable OPO and a time-resolved ICCD. The complex luminescence spectra of several REEs were studied and multiple suitable excitation wavelengths for detecting the REE^{3+} luminescence peaks from both apatite and calcite were presented. A broad band of Mn^{2+} was seen as a strong background, especially in calcite. For apatite, the luminescence of Eu^{3+} and Sm^{3+} occupying different Ca sites was observed with specific excitation regions, which would offer further information about the crystal structure. As a main result, the laser excitation region in deep UV around ~220–230 nm was discovered very promising. Within this range, the intensive luminescence of Tb^{3+} and Sm^{3+} was observed from both minerals and in the case of apatite peaks of $Nd^{3+}$and Eu^{3+} as occupying Ca (I) and Ca (II) sites were detected. In addition, the luminescence of Mn^{2+} is not strong with these excitations. Applicability of the optimized excitation wavelengths found here was demonstrated with a non-gated detector, as it would be more feasible for *in-situ* analysis of minerals.

Author statement

Sari Romppanen: Investigation, Resources, Software, Funding acquisition, Conceptualization, Visualization, Data Curation, Writing - Original Draft, Writing - Review & Editing. **Heikki Häkkänen**: Investigation, Resources, Software, Supervision, Funding acquisition, Conceptualization, Visualization, Writing - Review & Editing. **Saara Kaski**: Supervision, Funding acquisition, Conceptualization, Visualization, Project administration, Writing - Original Draft, Writing - Review & Editing.

Declaration of competing interest

The authors declare that they have no known competing financial interests or personal relationships that could have appeared to influence the work reported in this paper.

5 Acknowledgments

This study was partly supported by the Academy of Finland (Grant 281955 to S.K. and Grant 282240 to H.H.). S.R. wishes to acknowledge K.H. Renlund's Foundation for the grant which offered the possibility to finalize this work.

The apatite sample for the research was chosen from the samples kindly offered by Yara Suomi Oy and Pasi Heino and Aleksi Salo are appreciated for the co-operation. The Mn-bearing calcite sample from Siilinjärvi was from the collection offered by Geological Survey of Finland: Jari Nenonen and Satu Hietala are thanked for it.

Appendix A. Supplementary data

Supplementary data to this article can be found online at https://doi.org/10.1016/j.jlumin.2021.117929.

References

[1] R. Eggert, C. Wadia, C. Anderson, D. Bauer, F. Fields, L. Meinert, P. Taylor, Rare earths: market disruption, innovation, and global supply chains, Annu. Rev. Environ. Resour. 41 (2016) 199–222, https://doi.org/10.1146/annurev-environ-110615-085700.

[2] P. Henderson, General geochemical properties and abundances of the rare earth elements, in: P. Henderson (Ed.), Rare Earth Elem. Geochemistry, Elsevier Science Publishers B.V., 1984, pp. 1–32.

[3] G. Blasse, B.C. Grabmaier, Luminescent Materials, Springer-Verlag, Berlin/Heidelberg, 1994, https://doi.org/10.1007/978-3-642-79017-1.

[4] M. Gaft, R. Reisfeld, G. Panczer, Modern Luminescence Spectroscopy of Minerals and Materials, Springer, Heidelberg, 2005, https://doi.org/10.1007/b137490.

[5] L. Nasdala, J. Götze, J.M. Hanchar, M. Gaft, M.R. Krbetschek, Luminescence techniques in earth sciences, in: Spectrosc. Methods Mineral., Mineralogical Society of Great Britain and Ireland, Germany, 2004, pp. 43–91, https://doi.org/10.1180/EMU-notes.6.2.

[6] M. Gaft, R. Reisfeld, G. Panczer, P. Blank, G. Boulon, Laser-induced time-resolved luminescence of minerals, Spectrochim. Acta Part A Mol. Biomol. Spectrosc. 54 (1998) 2163–2175, https://doi.org/10.1016/S1386-1425(98)00134-6.

[7] P. Blanc, A. Baumer, F. Cesbron, D. Ohnenstetter, G. Panczer, G. Rémond, Systematic cathodoluminescence spectral analysis of synthetic doped minerals: anhydrite, apatite, calcite, fluorite, scheelite and zircon, in: Cathodoluminescence Geosci., Springer Berlin Heidelberg, 2000, pp. 127–160, https://doi.org/10.1007/978-3-662-04086-7_5.

[8] J. Götze, Application of cathodoluminescence microscopy and spectroscopy in geosciences, Microsc. Microanal. 18 (2012) 1270–1284, https://doi.org/10.1017/S1431927612001122.

[9] H. Friis, Luminescence Spectroscopy of Natural and Synthetic REE-Bearing Minerals, University of St. Andrews, 2009.

[10] S. Boggs, D. Krinsley, Application of Cathodoluminescence Imaging to the Study of Sedimentary Rocks, Cambridge University Press, 2006, https://doi.org/10.1017/cbo9780511535475.

[11] M. Pagel, V. Barbin, P. Blanc, D. Ohnenstetter (Eds.), Cathodoluminescence in Geosciences, Springer, Berlin, Heidelberg, 2000, https://doi.org/10.1007/978-3-662-04086-7.

[12] M. Gaft, R. Reisfeld, G. Panczer, Modern Luminescence Spectroscopy of Minerals and Materials, second ed., Springer Mineralogy, 2015 https://doi.org/10.1007/978-3-319-24765-6.

[13] M. Gaft, G. Panczer, R. Reisfeld, E. Uspensky, Laser-induced time-resolved luminescence as a tool for rare-earth element identification in minerals, Phys. Chem. Miner. 28 (2001) 347–363, https://doi.org/10.1007/s002690100163.

[14] M. Gaft, G. Panczer, Laser-induced time-resolved luminescence spectroscopy of minerals: a powerful tool for studying the nature of emission centres, Mineral. Petrol. 107 (2013) 363–372, https://doi.org/10.1007/s00710-013-0293-3.

[15] T. Al-Ani, F. Molnár, P. Lintinen, S. Leinonen, T. Al-Ani, F. Molnár, P. Lintinen, S. Leinonen, Geology and mineralogy of rare earth elements deposits and occurrences in Finland, Minerals 8 (2018) 356, https://doi.org/10.3390/min8080356.

[16] K. Puustinen, Geology of the Siilinjärvi Carbonatite Complex, Eastern Finland, Geologinen tutkimuslaitos, Otaniemi, 1971.

[17] I. Hornig-Kjarsgaard, Rare earth elements in sovitic carbonatites and their mineral phases, J. Petrol. 39 (1998) 2105–2121, https://doi.org/10.1093/petroj/39.11-12.2105.

[18] W.A. Deer, R.A. Howi, J. Zussman, An Introduction to the Rock-Forming Minerals, third ed., Mineralogical Society of Great Britain and Ireland, 2013 https://doi.org/10.1180/DHZ.

[19] G.A. Waychunas, Apatite luminescence, Rev. Mineral. Geochem. 48 (2002) 701–742, https://doi.org/10.2138/rmg.2002.48.19.

[20] J.-M. Baele, R. Dreesen, M. Dusar, Assessing apatite cathodoluminescence as a tool for sourcing oolitic ironstones 126 (2015) 57–67.

[21] J. Barbarand, M. Pagel, Cathodoluminescence study of apatite crystals, Am. Mineral. 86 (2001) 473–484, https://doi.org/10.2138/am-2001-0411.

[22] J.M. Hughes, J. Rakovan, The crystal structure of apatite, Ca5(PO4)3(F,OH,Cl), Rev. Mineral. Geochem. 48 (2002) 1–12, https://doi.org/10.2138/rmg.2002.48.1.

[23] J.M. Hughes, M. Cameron, K.D. Crowley, Structural variations in natural F, OH, and Cl apatites, Am. Mineral. 74 (1989) 870–876.

[24] G. Blasse, Influence of local charge compensation on site occupation and luminescence of apatites, J. Solid State Chem. 14 (1975) 181–184, https://doi.org/10.1016/0022-4596(75)90009-2.

[25] J.M. Hughes, M. Cameron, A. Mariano, Rare-earth-element ordering and structural variations in natural rare-earth'bearing apatites, Am. Mineral. 76 (1991) 1165–1173.

[26] M.E. Fleet, Y. Pan, Site preference of rare earth elements in fluorapatite, Am. Mineral. 80 (1995) 329–335, https://doi.org/10.2138/am-1995-3-414.

[27] M.E. Fleet, Y. Pan, Crystal chemistry of Rare Earth Elements in fluorapatite and some calc-silicates, Eur. J. Mineral 7 (1995) 591–606, https://doi.org/10.1127/ejm/7/3/0591.

[28] M.E. Fleet, Yuanming Pan, Site preference of rare earth elements in fluorapatite: binary (LREE+HREE)-substituted crystals, Am. Mineral. 82 (1997) 870–877, https://doi.org/10.2138/am-1997-9-1004.

[29] G. Chazot, M.A. Menzies, B. Harte, Determination of partition coefficients between apatite, clinopyroxene, amphibole, and melt in natural spinel Iherzolites from Yemen: implications for wet melting of the lithospheric mantle, Geochem. Cosmochim. Acta 60 (1996) 423–437, https://doi.org/10.1016/0016-7037(95)00412-2.

[30] R.A. Mason, A.N. Mariano, Cathodoluminescence activation in manganese-bearing and rare earth-bearing synthetic calcites, Chem. Geol. 88 (1990) 191–206, https://doi.org/10.1016/0009-2541(90)90113-L.

[31] G. Blasse, M. Aguilar, Luminescence of natural calcite (CaCO3), J. Lumin. 29 (1984) 239–241, https://doi.org/10.1016/S0022-2313(84)90091-7.

[32] D. Habermann, R.D. Neuser, D.K. Richter, REE-activated cathodoluminescence of calcite and dolomite: high-resolution spectrometric analysis of CL emission (HRS-CL), Sediment, Geol. 101 (1996) 1–7, https://doi.org/10.1016/0037-0738(95)00086-0.

[33] M.B. Toffolo, G. Ricci, L. Caneve, I. Kaplan-Ashiri, Luminescence reveals variations in local structural order of calcium carbonate polymorphs formed by different mechanisms, Sci. Rep. 9 (2019) 1, https://doi.org/10.1038/s41598-019-52587-7.

[34] M. Gaft, L. Nagli, G. Panczer, G. Waychunas, N. Porat, The nature of unusual luminescence in natural calcite CaCO3, Am. Mineral. 93 (2008) 158–167, https://doi.org/10.2138/am.2008.2576.

[35] S. Bodył, Luminescence properties of Ce3+ and Eu2+ in fluorites and apatites, Mineralogia 40 (2009) 85–94, https://doi.org/10.2478/v10002-009-0007-y.

[36] R. Reisfeld, M. Gaft, G. Boulon, C. Panczer, C.K. Jørgensen, Laser-induced luminescence of rare-earth elements in natural fluor-apatites, J. Lumin. 69 (1996) 343–353, https://doi.org/10.1016/S0022-2313(96)00114-7.

[37] S.E. Sommer, Cathodoluminescence of carbonates, 2, Geological applications, Chem. Geol. 9 (1972) 275–284, https://doi.org/10.1016/0009-2541(72)90065-4.

[38] A. El Ali, V. Barbin, G. Calas, B. Cervelle, K. Ramseyer, J. Bouroulec, Mn2+-activated luminescence in dolomite, calcite and magnesite: quantitative determination of manganese and site distribution by EPR and CL spectroscopy, Chem. Geol. 104 (1993) 189–202, https://doi.org/10.1016/0009-2541(93)90150-H.

[39] A. Sidike, X.M. Wang, A. Sawuti, H.J. Zhu, I. Kusachi, N. Yamashita, Energy transfer among Pb, Ce and Mn in fluorescent calcite from Kuerle, Xinjiang, China, Phys. Chem. Miner. 33 (2006) 559–566, https://doi.org/10.1007/s00269-006-0103-0.

[40] D. Habermann, R.D. Neuser, D.K. Richter, Low limit of Mn2+-activated cathodoluminescence of calcite: state of the art, Sediment. Geol. 116 (1998) 13–24, https://doi.org/10.1016/S0037-0738(97)00118-8.

[41] V.A. Pedone, K.R. Cercone, R.C. Burruss, Activators of photoluminescence in calcite: evidence from high-resolution, laser-excited luminescence spectroscopy, Chem. Geol. 88 (1990) 183–190, https://doi.org/10.1016/0009-2541(90)90112-K.

[42] G. Walker, O.E. Abumere, B. Kamaluddin, Luminescence spectroscopy of Mn2+ centres in rock-forming carbonates, Mineral. Mag. 53 (1989) 201–211, https://doi.org/10.1180/minmag.1989.053.370.07.

[43] H.G. Machel, R.A. Mason, A.N. Mariano, A. Mucci, Causes and emission of luminescence in calcite and dolomite, in: H.Y.C. Charles E. Barker, Robert C. Burruss, Otto C. Kopp, Hans G. Machel, Donald J. Marshall, Paul Wright (Eds.), Lumin. Microsc. Spectrosc. Qual. Quant. Appl., SEPM Society for Sedimentary Geology, 1991, https://doi.org/10.2110/scn.91.25.0009.

[44] U. Kempe, J. Götze, Cathodoluminescence (CL) behaviour and crystal chemistry of apatite from rare-metal deposits, Mineral. Mag. 66 (2002) 151–172, https://doi.org/10.1180/0026461026610019.

[45] M. Gaft, R. Reisfeld, G. Panczer, G. Boulon, S. Shoval, B. Champagnon, Accommodation of rare-earths and manganese by apatite, Opt. Mater. 8 (1997) 149–156, https://doi.org/10.1016/S0925-3467(97)00042-6.

[46] K. Linganna, S. Ju, C. Basavapoornima, V. Venkatramu, C.K. Jayasankar, Journal of Asian Ceramic Societies Luminescence and decay characteristics of Tb 3+-doped fluorophosphate glasses Luminescence and decay characteristics of Tb 3+-doped fluorophosphate glasses, J. Asian Ceram. Soc. 6 (2018) 82–87, https://doi.org/10.1080/21870764.2018.1442674.

[47] T.H. Tran, K.A. Tran, T.K. Hoang, T.H. Pham, Q.M. Le, Fabrication and properties of terbium phosphate nanorods, Adv. Nat. Sci. Nanosci. Nanotechnol. 3 (2012), https://doi.org/10.1088/2043-6262/3/1/015010, 015010.

[48] T. Hayakawa, N. Kamata, K. Yamada, Visible emission characteristics in Tb3+-doped fluorescent glasses under selective excitation, J. Lumin. 68 (1996) 179–186, https://doi.org/10.1016/0022-2313(96)00022-1.

[49] M. Nazarov, E.J. Popovici, I. Arellano, D.Y. Noh, Luminescence properties of europium and terbium activated yttrium niobium/tantalate phosphors under VUV-UV excitation, Mold. J. Phys. Sci. 7 (2008) 433–437.

[50] H. Zhu, B. Qian, X. Zhou, Y. Song, K. Zheng, Y. Sheng, H. Zou, Tunable luminescence and energy transfer of Tb3+/Eu3+ co-doped cubic CaCO3 nanoparticles, J. Lumin. 203 (2018) 441–446, https://doi.org/10.1016/j.jlumin.2018.06.041.

[51] M.A. Mickens, Z. Assefa, Tunable luminescence and white light emission of novel multiphase sodium calcium silicate nanophosphors doped with Ce3+, Tb3+, and Mn2+ ions, J. Lumin. 145 (2014) 498–506, https://doi.org/10.1016/j.jlumin.2013.07.053.

[52] J.F.M. dos Santos, N.G.C. Astrath, M.L. Baesso, L.A.O. Nunes, T. Catunda, The effect of silica content on the luminescence properties of Tb3+-doped calcium aluminosilicate glasses, J. Lumin. 202 (2018) 363–369, https://doi.org/10.1016/j.jlumin.2018.05.008.

[53] C.J. Duan, W.F. Li, X.Y. Wu, H.H. Chen, X.X. Yang, J.T. Zhao, Y.B. Fu, Z.M. Qi, G. Bin Zhang, Z.S. Shi, Photoluminescence of Ce3+, Tb3+, Sm3+ or Gd3+ activated Ba3BP3O12 under the VUV and UV excitation, Mater. Sci. Eng. B Solid-State Mater. Adv. Technol. 121 (2005) 272–277, https://doi.org/10.1016/j.mseb.2005.04.013.

[54] F. Meng, X. Zhang, Y. Xu, J. Yang, Z. Cheng, Photoluminescence of Eu2+, Ce3+ and Tb3+ in a new potassium barium phosphate K2Ba3(P2O7)2 host lattice, J. Alloys Compd. (2017), https://doi.org/10.1016/j.jallcom.2017.09.224.

[55] H. Desirena, J. Molina-González, O. Meza, P. Castillo, J. Bujdud-Pérez, Multicolor and warm white emissions with a high color rendering index in a Tb3+/Eu3+-codoped phosphor ceramic plate, Materials 12 (2019) 2240, https://doi.org/10.3390/ma12142240.

[56] W. Chen, R. Sammynaiken, Y. Huang, Photostimulated luminescence of Tb3+ and Eu 3+ in zeolite-Y, Lumin, Solids J. Chem. Phys. 88 (2000) 836, https://doi.org/10.1063/1.373834.

[57] A. Akrim, D. Zambon, J.C. Cousseins, Optical properties of Tb3+ in the diphosphate CsYP2O7, J. Alloys Compd. 207–208 (1994) 99–101, https://doi.org/10.1016/0925-8388(94)90186-4.

[58] C.A. Kodaira, H.F. Brito, E.E.S. Teotonio, M.C.F.C. Felinto, O.L. Malta, G.E. S. Brito, Photoluminescence behavior of the Sm3+ and Tb3+ ions doped into the Gd2(WO4)3 matrix prepared by the Pechini and ceramic methods, J. Braz. Chem. Soc. 15 (2004) 890–896, https://doi.org/10.1590/S0103-50532004000600016.

[59] W.A. Pisarski, L. Zur, M. Sołtys, J. Pisarska, Terbium-terbium interactions in lead phosphate glasses, J. Appl. Phys. 113 (2013), https://doi.org/10.1063/1.4799592.

[60] G. Ju, Y. Hu, L. Chen, Y. Jin, Z. Yang, T. Wang, Photoluminescence properties of Ce3+and Tb3+-activated Ba2Mg(PO4)2, Opt. Mater. Express 5 (2015) 1, https://doi.org/10.1364/ome.5.000001.

[61] R.H. Mitchell, J. Xiong, A.N. Mariano, M.E. Fleet, Rare-earth-element-activated cathodoluminescence in apatite, Can. Mineral. 35 (1997) 979–998.

[62] M. Czaja, S. Bodył, R. Lisiecki, Z. Mazurak, Luminescence properties of Pr3+ and Sm3+ ions in natural apatites, Phys. Chem. Miner. 37 (2010) 425–433, https://doi.org/10.1007/s00269-009-0344-9.

[63] N.P.O. Homman, C. Yang, K.G. Malmqvist, A highly sensitive method for rare-earth element analysis using ionoluminescence combined with PIXE, Nucl. Instrum. Methods Phys. Res. A. 353 (1994) 610–614, https://doi.org/10.1016/0168-9002(94)91734-5.

[64] D. Habermann, J. Meijer, R.D. Neuser, D.K. Richter, C. Rolfs, A. Stephan, Micro-PIXE and quantitative cathodoluminescence spectroscopy: combined high resolution trace element analyses in minerals, Nucl. Instrum. Methods Phys. Res. Sect. B Beam Interact. Mater. Atoms 150 (1999) 470–477, https://doi.org/10.1016/S0168-583X(98)00926-4.

[65] H.M. Farok, G.A. Saunders, W. Poon, H. Vass, Low temperature fluorescence, valence state and elastic anomalies of samarium phosphate glasses, J. Non-Cryst. Solids 142 (1992) 175–180, https://doi.org/10.1016/S0022-3093(05)80022-5.

[66] K. Annapurna, R.N. Dwivedi, P. Kundu, S. Buddhudu, Fluorescence properties of Sm3+: ZnCl2-BaCl2-LiCl glass, Mater. Res. Bull. 38 (2003) 429–436, https://doi.org/10.1016/S0025-5408(02)01068-1.

[67] Y. Wen, Y. Wang, B. Liu, F. Zhang, Luminescence properties of Ca4Y6(SiO4)6O: RE3+ (RE = Eu, Tb, Dy, Sm and Tm) under vacuum ultraviolet excitation, Opt. Mater. 34 (2012) 889–892, https://doi.org/10.1016/J.OPTMAT.2011.12.005.

[68] Z. Yang, D. Xu, J. Sun, Synthesis and Luminescence Properties of Ba3Lu(PO4)3: Sm3+ phosphor for white light- emitting diodes, Optic Express 25 (2017), https://doi.org/10.1364/OE.25.00A391. A391–A401.

[69] F.S. Liu, Q.L. Liu, J.K. Liang, J. Luo, L.T. Yang, G.B. Song, Y. Zhang, L.X. Wang, J. N. Yao, G.H. Rao, Optical spectra of Ln3+(Nd3+, Sm3+, Dy3+, Ho3+, Er3+)-doped Y3GaO6, J. Lumin. 111 (2005) 61–68, https://doi.org/10.1016/J.JLUMIN.2004.06.005.

[70] C.K. Jayasankar, P. Babu, Optical properties of Sm3+ ions in lithium borate and lithium fluoroborate glasses, J. Alloys Compd. 307 (2000) 82–95, https://doi.org/10.1016/S0925-8388(00)00888-4.

[71] S. Bodył, M. Czaja, Z. Mazurak, Optical properties of Pr3+, Sm3+ and Er3+ ions in apatite, fluorite and phosphate glasses, Phys. Procedia. 2 (2009) 515–525, https://doi.org/10.1016/j.phpro.2009.07.037.

[72] B.V. Rao, U. Rambabu, S. Buddhudu, Emission analysis of Sm3+:Ca4GdO(BO3)3 powder phosphor, Mater. Lett. 61 (2007) 2868–2871, https://doi.org/10.1016/j.matlet.2007.01.042.

[73] G.S.R. Raju, S. Buddhudu, Emission analysis of Sm3+ and Dy3+:MgLaLiSi2O7 powder phosphors, Spectrochim. Acta Part A Mol. Biomol. Spectrosc. 70 (2008) 601–605, https://doi.org/10.1016/J.SAA.2007.08.004.
[74] R. Jagannathan, M. Kottaisamy, Eu3+ luminescence: a spectral probe in M5(PO4) 3X apatites, (M = Ca or Sr; X = F–, Cl–, Br– or OH–), J. Phys. Condens. Matter 7 (1995) 8453–8466, https://doi.org/10.1088/0022-3727/27/10/034.
[75] M. Gaft, R. Reisfeld, G. Panczer, S. Shoval, C. Garapon, G. Boulon, W. Strek, Luminescence of Eu(III), Pr(III) and Sm(III) in carbonate-fluor-apatite, Acta Phys. Pol. Ser. A. 90 (1996) 267–274.
[76] R. Ternane, M. Trabelsi-Ayedi, N. Kbir-Ariguib, B. Piriou, Luminescent properties of Eu3+ in calcium hydroxyapatite, J. Lumin. 81 (1999) 165–170, https://doi.org/10.1016/S0022-2313(98)00172-0.
[77] M. Gaft, R. Reisfeld, G. Panczer, S. Shoval, B. Champagnon, G. Boulon, Eu3+ luminescence in high-symmetry sites of natural apatite, J. Lumin. 72–74 (1997) 572–574, https://doi.org/10.1016/S0022-2313(96)00229-3.
[78] B. Piriou, D. Fahmi, J. Dexpert-Ghys, A. Taitai, J.L. Lacout, Unusual fluorescent properties of Eu3+ in oxyapatites, J. Lumin. 39 (1987) 97–103, https://doi.org/10.1016/0022-2313(87)90036-6.
[79] B. Piriou, A. Elfakir, M. Quarton, Site-selective spectroscopy of Eu3+-doped sodium lead phosphate apatite, J. Lumin. 93 (2001) 17–26, https://doi.org/10.1016/S0022-2313(01)00172-7.
[80] A. Zounani, D. Zambon, J.C. Cousseins, Spectroscopic study of Eu3+ in the fluorapatite Sr10F2(PO4)6, J. Alloys Compd. 207–208 (1994) 94–98, https://doi.org/10.1016/0925-8388(94)90185-6.
[81] A. Zounani, D. Zambon, J.C. Cousseins, Optical properties of Eu3+ activated Sr10F2(PO4)6 elaborated by coprecipitation, J. Alloys Compd. 188 (1992) 82–86, https://doi.org/10.1016/0925-8388(92)90648-S.
[82] F. Nouri, G. Panczer, Y. Guyot, M. Trabelsi-Ayadi, R. Ternane, Synthesis and luminescent properties of Eu3+-doped phosphate-sulfate fluorapatites Ca10−xNax(PO4)6−x(SO4)xF2, J. Lumin. 192 (2017) 590–594, https://doi.org/10.1016/j.jlumin.2017.07.033.
[83] V. Jokanović, B. Čolović, N. Jović, The luminescent properties of yttrium oxyapatite doped with Eu 3+ ions, Sci. Sinter. 46 (2014) 129–134, https://doi.org/10.2298/SOS1401129J.
[84] A. Tesch, C. Wenisch, K.H. Herrmann, J.R. Reichenbach, P. Warncke, D. Fischer, F.A. Müller, Luminomagnetic Eu3+ - and Dy3+ -doped hydroxyapatite for multimodal imaging, Mater. Sci. Eng. C 81 (2017) 422–431, https://doi.org/10.1016/j.msec.2017.08.032.
[85] M. Gaft, R. Reisfeld, G. Panczer, O. Ioffe, I. Sigal, Laser-induced time-resolved luminescence as a means for discrimination of oxidation states of Eu in minerals, J. Alloys Compd. 323–324 (2001) 842–846, https://doi.org/10.1016/S0925-8388(01)01157-4.
[86] R. El Ouenzerfi, N. Kbir-Ariguib, M. Trabelsi-Ayedi, B. Piriou, Spectroscopic study of Eu3+ in strontium hydroxyapatite Sr10(PO4)6(OH)2, J. Lumin. 85 (1999) 71–77, https://doi.org/10.1016/S0022-2313(99)00149-0.
[87] M. Marques Fernandes, M. Schmidt, T. Stumpf, C. Walther, D. Bosbach, R. Klenze, T. Fanghänel, Site-selective time-resolved laser fluorescence spectroscopy of Eu3 + in calcite, J. Colloid Interface Sci. (2008), https://doi.org/10.1016/j.jcis.2008.01.017.
[88] B. Piriou, M. Fedoroff, J. Jeanjean, L. Bercis, Characterization of the sorption of europium(lll) on calcite by site-selective and time-resolved luminescence spectroscopy, J. Colloid Interface Sci. (1997), https://doi.org/10.1006/jcis.1997.5115.
[89] K. Binnemans, Interpretation of europium(III) spectra, Coord. Chem. Rev. 295 (2015) 1–45, https://doi.org/10.1016/J.CCR.2015.02.015.
[90] Y. Il Jeon, L. Krishna Bharat, J.S. Yu, Synthesis and luminescence properties of Eu3+/Dy3+ ions co-doped Ca2La8(GeO4)6O2 phosphors for white-light applications, J. Alloys Compd. 620 (2015) 263–268, https://doi.org/10.1016/j.jallcom.2014.09.135.
[91] T.B. de Queiroz, M.B.S. Botelho, T.S. Gonçalves, M.R. Dousti, A.S.S. de Camargo, New fluorophosphate glasses co-doped with Eu3+ and Tb3+ as candidates for generating tunable visible light, J. Crit. Care 38 (2015) 315–321, https://doi.org/10.1016/j.jallcom.2015.06.066.
[92] Y.N. Xue, F. Xiao, Q.Y. Zhang, Enhanced red light emission from LaBSiO5:Eu3+, R3+ (R = Bi or Sm) phosphors, Spectrochim. Acta Part A Mol. Biomol. Spectrosc. 78 (2011) 607–611, https://doi.org/10.1016/J.SAA.2010.11.030.
[93] M. Gaft, R. Reisfeld, G. Panczer, E. Uspensky, B. Varrel, G. Boulon, Luminescence of Pr3+ in minerals, Opt. Mater. 13 (1999) 71–79, https://doi.org/10.1016/S0925-3467(99)00014-2.
[94] M. Czaja, R. Lisiecki, Luminescence of agrellite specimen from the kipawa river locality, Minerals 9 (2019) 752, https://doi.org/10.3390/min9120752.
[95] M.B. Czaja, S. Bodył-Gajowska, Z. Mazurak, Steady-state luminescence measurement for qualitative identification of rare earth ions in minerals, J. Mineral. Petrol. Sci. 108 (2013) 47–54, https://doi.org/10.2465/jmps.111229.
[96] M. Gaft, Y. Raichlin, Luminescence of 5d–4f transitions of Pr3+ in natural fluorite CaF2, anhydrite CaSO4 and apatite Ca5(PO4)3F, Phys. Chem. Miner. 47 (2020) 1–8, https://doi.org/10.1007/s00269-019-01074-6.
[97] M. Soltys, L. Żur, J. Pisarska, W.A. Pisarski, Excitation and luminescence of Dy3+ ions in PbO-P2O5-Ga2O3 glass system, J. Rare Earths 32 (2014) 213–216, https://doi.org/10.1016/S1002-0721(14)60054-5.
[98] M. Seshadri, K. Venkata Rao, J. Lakshmana Rao, K.S.R. Koteswara Rao, Y. C. Ratnakaram, Spectroscopic investigations and luminescence spectra of Nd3+ and Dy3+ doped different phosphate glasses, J. Lumin. 130 (2010) 536–543, https://doi.org/10.1016/J.JLUMIN.2009.10.027.
[99] V.K. Rai, S.B. Rai, D.K. Rai, Optical studies of Dy3+ doped tellurite glass: observation of yellow-green upconversion, Optic Commun. 257 (2006) 112–119, https://doi.org/10.1016/j.optcom.2005.07.022.
[100] W.Y. Zhao, S.L. An, B. Fan, S.B. Li, Y.T. Dai, Photoluminescence and cathodoluminescence properties of a novel CaLaGa3O7:Dy3+ phosphor, Chin. Sci. Bull. 57 (2012) 827–831, https://doi.org/10.1007/s11434-011-4938-5.
[101] M. Suta, Ž. Antić, V. Đorđević, S. Kuzman, M.D. Dramićanin, A. Meijerink, Making Nd3+ a sensitive luminescent thermometer for physiological temperatures—an account of pitfalls in Boltzmann thermometry, Nanomaterials 10 (2020) 543, https://doi.org/10.3390/nano10030543.
[102] Y.C. Ratnakaram, N.V. Srihari, A.V. Kumar, D.T. Naidu, R.P.S. Chakradhar, Optical absorption and photoluminescence properties of Nd3+ doped mixed alkali phosphate glasses-spectroscopic investigations, Spectrochim. Acta Part A Mol. Biomol. Spectrosc. 72 (2009) 171–177, https://doi.org/10.1016/J.SAA.2008.09.008.
[103] D. de Ligny, G. Panczer, D. Caurant, D.R. Neuville, Contribution of neodymium optical spectroscopy to the crystal growth study of a silicate apatite in a glassy matrix, Opt. Mater. 30 (2008) 1694–1698, https://doi.org/10.1016/j.optmat.2007.07.008.
[104] J.B. Gruber, C.A. Morrison, M.D. Seltzer, A.O. Wright, M.P. Nadler, T.H. Allik, J. A. Hutchinson, B.H.T. Chai, Site-selective excitation and polarized absorption spectra of Nd3+ in Sr5(PO4)3F and Ca5(PO4)3F, J. Appl. Phys. 79 (1996) 1746–1758, https://doi.org/10.1063/1.360964.
[105] S. Damodaraiah, V. Reddy Prasad, Y.C. Ratnakaram, Investigations on spectroscopic properties of Nd3+ doped alkali bismuth phosphate glasses for 1.053 μm laser applications, Optic Laser. Technol. 113 (2019) 322–329, https://doi.org/10.1016/J.OPTLASTEC.2019.01.010.
[106] G. Lakshminarayana, R. Vidya Sagar, S. Buddhudu, NIR luminescence from Er3+/Yb3+, Tm3+/Yb3+, Er3+/Tm3+ and Nd3+ ions-doped zincborotellurite glasses for optical amplification, J. Lumin. 128 (2008) 690–695, https://doi.org/10.1016/J.JLUMIN.2007.11.081.
[107] C. Lenz, D. Talla, K. Ruschel, R. Škoda, J. Götze, L. Nasdala, Factors affecting the Nd3+ (REE3+) luminescence of minerals, Mineral. Petrol. 107 (2013) 415–428, https://doi.org/10.1007/s00710-013-0286-2.